JOURNAL OF GUIDANCE, CONTROL, AND DYNAMICS
Vol. 26, No. 2, March–April 2003

Spacecraft Attitude Rate Estimation from Geomagnetic Field Measurements

Mark L. Psiaki*
Cornell University, Ithaca, New York 14853-7501
and
Yaakov Oshman†
Technion—Israel Institute of Technology, 32000 Haifa, Israel

Methods are developed for estimating the rotation rate of a spacecraft using only measured magnetic field data. The goal is to provide rate information for use in applications such as detumbling, nutation damping, and momentum management without using gyroscopes. Two algorithms are developed, a deterministic algorithm and an extended Kalman filter. Both algorithms employ the magnetic field direction kinematics equation and Euler's equation for attitude motion of a rigid body with momentum wheels. Neither algorithm requires a model of the Earth's magnetic field. The deterministic algorithm solves a nonlinear least-squares problem for the unknown angular momentum component along the magnetic field direction. The extended Kalman filter estimates the attitude rate vector, corrections to five of the six inertia matrix elements, and two error states of the measured magnetic field direction. It uses an initial rate estimate from the deterministic algorithm to avoid divergence. The algorithms have been tested using data from a spinning sounding rocket. They achieve initial accuracies in the range 2–7 deg/s when the rocket spins at about 80 deg/s, and their accuracies improve to 1–2 deg/s after the spin rate decays to 20 deg/s. These results indicate a lower bound on the ratio of the error to the nominal spin rate, which suggests that dynamic modeling error is the dominant source of uncertainty.

I. Introduction

MANY spacecraft need estimates of their rotation rates. The spin rate may be used to apply a control that stops tumbling, to manage the total system angular momentum, to aid a star tracker, or as part of an attitude determination system. The most common method of determining attitude rate is by direct rate-gyro measurement. This paper develops two attitude rate estimation methods that rely on Earth magnetic field measurements rather than on rate-gyro measurements.

There are several important reasons to avoid the use of rate gyros. Gyros are expensive and failure prone. They have significant mass and consume a significant amount of power. The desire to manufacture small, lightweight, inexpensive, and reliable satellites militates against the use of rate gyros. Gyroless rate estimation schemes can be important even for missions that include rate gyros because these schemes provide a backup capability.

A number of methods have been developed to estimate attitude rate without using rate-gyro data. Some methods work directly with vector attitude data and use either deterministic differentiation techniques or Kalman filtering techniques to estimate attitude rate (see Refs. 1–3). Another method uses full three-axis attitude estimates as inputs to a rate estimation filter.[4] In Ref. 5, both types of measurements are considered and filters are compared to derivative-based estimators. Another class of methods estimates attitude and attitude rate simultaneously, using vector and scalar attitude measurements. These include deterministic methods that employ differentiation techniques[6,7] and filter-based techniques.[6–10]

A unique aspect of the rate estimation techniques described in Ref. 3 is the complete lack of dependence on attitude knowledge. The techniques' algorithms assume that the measured attitude reference vector is fixed in inertial space, so that there is no need to transform an inertial time derivative into body coordinates. The only other known gyroless rate estimation algorithm that is independent of attitude knowledge is the high-rate limit algorithm of Ref. 7. Attitude-independent rate estimation techniques are suitable for applications such as detumbling control, momentum management, or nutation damping, but their outputs are not sufficiently accurate to be used like rate gyros in an attitude estimation filter.

In Ref. 3, the attitude rate is estimated by the use of a time series of measurements of the Earth's magnetic field vector. The methods do not require knowledge of the magnetic field direction in inertial coordinates. This feature allows the estimators to work without spacecraft position knowledge and without a complicated spherical harmonic model of the Earth's magnetic field. This attitude reference vector, however, has a nonzero inertial rotation rate as a spacecraft moves along its orbit, which violates the paper's assumption. Fortunately, this rotation rate is normally less than 0.12 deg/s, which implies that the method can work effectively if the required attitude rate resolution is no finer than this lower bound.

In Refs. 3, 6, and 7, nonlinearities are handled by the use of deterministic batch algorithms in conjunction with extended Kalman filters. The batch algorithms deal directly with nonlinearities and cannot diverge. Their outputs are used to initialize extended Kalman filters (EKF) near enough to the true state to avoid divergence. The techniques described in Refs. 1, 2, and 4, on the other hand, use unusual Kalman filters that try to maintain linearity by making approximations. These methods do not require special algorithms for initialization because they are less prone to diverge, but their estimates are likely to be less accurate than those of a converged EKF.

The present paper develops improved versions of the two rate estimation algorithms described in Ref. 3. The new deterministic algorithm works directly with Euler's equation to determine the attitude rate along the magnetic field direction, and it uses an improved solution technique that incorporates a global nonlinear least-squares solver. The new Kalman filter improves on the Ref. 3 filter by explicitly accounting for the normalization constraint on the measured magnetic field direction vector. It also augments the filter state to include five of the six inertia matrix elements. The Ref. 3 techniques were tested using only simulated data, but the present improvements

Received 30 November 2001; revision received 13 May 2002; accepted for publication 11 November 2002.

*Associate Professor, Sibley School of Mechanical and Aerospace Engineering. Associate Fellow AIAA.

†Associate Professor, Department of Aerospace Engineering. Member, Asher Space Research Institute. Associate Fellow AIAA.

enable their approach to work well with actual flight data from a spinning spacecraft.

This paper's methods and results are presented in the next five sections. In Sec. II, dynamic models of the attitude rate vector and of the magnetic field direction vector are presented. These models are used to develop the two attitude rate estimation algorithms. The deterministic attitude rate estimator is developed in Sec. III. In Sec. IV, the observability of the system is analyzed and the rare conditions under which the attitude rate cannot be estimated based on magnetic field measurements alone is determined. The EKF attitude rate estimator is described in Sec. V. In Sec. VI, the results of tests of the two algorithms on actual flight data are presented. The paper's conclusions are presented in Sec. VII.

II. Dynamic Models for the Attitude Rate and Magnetic Field Direction Vectors

A. Rigid-Body Attitude Dynamics Model

Both of the rate estimators use Euler's equations to model the attitude rate vector's dynamics. The model includes a main rigid body and momentum wheels. It takes the form

$$I_m\dot{\boldsymbol{\omega}} + \dot{\boldsymbol{h}} + \boldsymbol{\omega} \times (I_m\boldsymbol{\omega} + \boldsymbol{h}) = \boldsymbol{w}_n \tag{1}$$

In this equation, I_m is the mass moment of inertia matrix, $\boldsymbol{\omega}$ is the angular velocity vector, $\boldsymbol{h}$ is the angular momentum vector of the momentum wheels, and $\boldsymbol{w}_n$ is the net external torque. All of these quantities are defined in spacecraft-fixed coordinates.

Two different models of the net external torque are used for the two different estimation algorithms. The deterministic algorithm assumes that $\boldsymbol{w}_n = 0$. The Kalman filter models $\boldsymbol{w}_n(t)$ as being a white-noise process disturbance. These assumptions could be relaxed to include explicit external torque models, but such models would complicate the estimation algorithms. Fortunately, external torques can be neglected or modeled as white noise in many circumstances without seriously degrading the attitude rate estimation accuracy.

B. Magnetic Field Kinematic Model

The estimation algorithms use a kinematic model of the motion of the magnetic field unit direction vector. Its takes the form

$$\dot{\hat{\boldsymbol{b}}} + \boldsymbol{\omega} \times \hat{\boldsymbol{b}} = -\boldsymbol{w}_\omega \times \hat{\boldsymbol{b}} \tag{2}$$

In this equation, $\hat{\boldsymbol{b}}$ is the body-axes magnetic field direction vector, and the vector $\boldsymbol{w}_\omega$ is the rotation rate of the magnetic field direction vector as measured with respect to inertial coordinates. All of these vectors are expressed in spacecraft body coordinates.

The two estimation algorithms use two different models for $\boldsymbol{w}_\omega$. The deterministic algorithm assumes that $\boldsymbol{w}_\omega = 0$. In a typical low Earth orbit, this assumption causes a maximum attitude rate error on the order of 0.12 deg/s because the magnetic field rotates with respect to inertial space at a rate of twice per orbit if the orbit passes over the magnetic poles. At lower magnetic inclinations, the field's inertial rotation rate is smaller, which reduces the error of assuming that $\boldsymbol{w}_\omega = 0$. The Kalman filter models $\boldsymbol{w}_\omega(t)$ as a white-noise process disturbance. This latter model allows for uncertainty about the field's slow inertial rotation rate and enables the filter to gradually deweight old magnetic field measurements.

C. Constant Projection of the Angular Momentum Along the Magnetic Field Direction

The deterministic algorithm assumes that the angular momentum vector and the magnetic field direction vector remain fixed in inertial space. This assumption is reasonable if the algorithm works with a short enough data batch because neither vector will have enough time to change significantly. This assumption implies that the projection of the angular momentum vector along the magnetic field direction is a constant, that is,

$$L_b = \hat{\boldsymbol{b}}^T(I_m\boldsymbol{\omega} + \boldsymbol{h}) \tag{3}$$

a scalar constant.

III. Deterministic Attitude Rate Estimation Algorithm

A. Two Components of Attitude Rate from Magnetic Field Kinematics

The magnetic field kinematics equation (2) can be used to determine the components of the attitude rate $\boldsymbol{\omega}$ that are perpendicular to the measured magnetic field. If one assumes that $\boldsymbol{w}_\omega = 0$, then Eq. (2) can be used to derive the following expression for the angular rate:

$$\boldsymbol{\omega} = \alpha\hat{\boldsymbol{b}} + \dot{\hat{\boldsymbol{b}}} \times \hat{\boldsymbol{b}} \tag{4}$$

where $\alpha = \hat{\boldsymbol{b}}^T\boldsymbol{\omega}$ is the unknown angular rate component parallel to the measured magnetic field direction. Equation (4) can be derived from Eq. (2) by taking the cross product of both sides of Eq. (2) with $\hat{\boldsymbol{b}}$ while recognizing that $(\boldsymbol{\omega} \times \hat{\boldsymbol{b}}) \times \hat{\boldsymbol{b}} = (\hat{\boldsymbol{b}}\hat{\boldsymbol{b}}^T - I)\boldsymbol{\omega}$, where I is the identity matrix.

The time derivative of $\hat{\boldsymbol{b}}$ is computed as follows. The actual measured data consist of $\boldsymbol{b}_0, \boldsymbol{b}_1, \boldsymbol{b}_2, \ldots$, a sequence of magnetic field vectors that are measured at the sample times $t_0, t_1, t_2, \ldots$. These raw measurements get processed using a batch curve fitting procedure that works with all of the measurements that fall within $\pm 0.5T_{\text{derv}}$ s of a given time of interest t_k. It fits each element of the measured field vector to a quadratic polynomial in t. These polynomials and their time derivative are used to produce smoothed estimates of $\boldsymbol{b}(t_k)$ and $\dot{\boldsymbol{b}}(t_k)$. The smoothed $\boldsymbol{b}(t_k)$ gets normalized to produce the $\hat{\boldsymbol{b}}_k$ value that is used in this paper's deterministic estimation algorithm. The time derivative of the normalization formula is used along with the smoothed $\dot{\boldsymbol{b}}(t_k)$ to compute $\dot{\hat{\boldsymbol{b}}}_k$. Care must be taken to use a reasonable length for the quadratic curve-fitting window T_{derv}. If T_{derv} is too large, then a quadratic model of $\boldsymbol{b}(t)$ will be poor, but if T_{derv} is too small, then the estimated $\dot{\hat{\boldsymbol{b}}}_k$ will be very noisy.

B. Parameterization of the Rate in Terms of an Angular Momentum Component

The unknown angular rate component α will be time varying in the general case. It is convenient to express $\alpha_k = \alpha(t_k)$ in terms of the constant angular momentum component along the magnetic field L_b. This can be accomplished by substituting the Eq. (4) expression for $\boldsymbol{\omega}$ into Eq. (3) and solving for α. The resulting formula is

$$\alpha_k = \frac{L_b - \hat{\boldsymbol{b}}_k^T\{I_m[\dot{\hat{\boldsymbol{b}}}_k \times \hat{\boldsymbol{b}}_k] + \boldsymbol{h}(t_k)\}}{\hat{\boldsymbol{b}}_k^T I_m \hat{\boldsymbol{b}}_k} \tag{5}$$

Equation (5) allows one to express the time-varying angular velocity in terms of the constant L_b. If one substitutes Eq. (5) into Eq. (4), the result is

$$\boldsymbol{\omega}_k = \boldsymbol{\omega}(t_k) = \boldsymbol{\gamma}_k + \boldsymbol{\eta}_k L_b \tag{6}$$

where the vectors $\boldsymbol{\gamma}_k$ and $\boldsymbol{\eta}_k$ are defined by the formulas

$$\boldsymbol{\gamma}_k = \dot{\hat{\boldsymbol{b}}}_k \times \hat{\boldsymbol{b}}_k - \hat{\boldsymbol{b}}_k\left[\frac{\hat{\boldsymbol{b}}_k^T\{I_m[\dot{\hat{\boldsymbol{b}}}_k \times \hat{\boldsymbol{b}}_k] + \boldsymbol{h}(t_k)\}}{\hat{\boldsymbol{b}}_k^T I_m \hat{\boldsymbol{b}}_k}\right] \tag{7a}$$

$$\boldsymbol{\eta}_k = \hat{\boldsymbol{b}}_k\left[\frac{1}{\hat{\boldsymbol{b}}_k^T I_m \hat{\boldsymbol{b}}_k}\right] \tag{7b}$$

Thus, the goal of estimating the attitude rate reduces to the goal of estimating the constant L_b.

C. Least-Squares Problem from Trapezoidal Integration of Euler's Equation

The unknown angular momentum component L_b can be determined by using Euler's equation (1). If one multiplies Eq. (1) by $(I_m)^{-1}$, integrates it trapezoidally from sample time t_k to sample time t_{k+1}, sets $\boldsymbol{w}_n = 0$, and uses Eq. (6) to eliminate ω_k and ω_{k+1} from the result, then the equation takes the following vector quadratic form:

$$\boldsymbol{c}_k L_b^2 + \boldsymbol{d}_k L_b + \boldsymbol{e}_k = 0 \tag{8}$$

where the vectors $\boldsymbol{c}_k$, $\boldsymbol{d}_k$, and $\boldsymbol{e}_k$ are defined by

$$\boldsymbol{c}_k = (\Delta t_k/2) I_m^{-1}[\boldsymbol{\eta}_{k+1} \times (I_m \boldsymbol{\eta}_{k+1}) + \boldsymbol{\eta}_k \times (I_m \boldsymbol{\eta}_k)] \tag{9a}$$

$$\begin{aligned}\boldsymbol{d}_k = {} & \boldsymbol{\eta}_{k+1} - \boldsymbol{\eta}_k + (\Delta t_k/2) I_m^{-1}\{\boldsymbol{\eta}_{k+1} \times [I_m \boldsymbol{\gamma}_{k+1} + \boldsymbol{h}(t_{k+1})] \\ & + \boldsymbol{\gamma}_{k+1} \times [I_m \boldsymbol{\eta}_{k+1}] + \boldsymbol{\eta}_k \times [I_m \boldsymbol{\gamma}_k + \boldsymbol{h}(t_k)] \\ & + \boldsymbol{\gamma}_k \times [I_m \boldsymbol{\eta}_k]\}\end{aligned} \tag{9b}$$

$$\begin{aligned}\boldsymbol{e}_k = {} & \boldsymbol{\gamma}_{k+1} - \boldsymbol{\gamma}_k + I_m^{-1}[\boldsymbol{h}(t_{k+1}) - \boldsymbol{h}(t_k)] + (\Delta t_k/2) I_m^{-1} \\ & \times \{\boldsymbol{\gamma}_{k+1} \times [I_m \boldsymbol{\gamma}_{k+1} + \boldsymbol{h}(t_{k+1})] + \boldsymbol{\gamma}_k \times [I_m \boldsymbol{\gamma}_k + \boldsymbol{h}(t_k)]\}\end{aligned} \tag{9c}$$

and where $\Delta t_k = t_{k+1} - t_k$ is the interval between the two sample times. The use of trapezoidal integration to derive Eq. (8) implies that Δt_k must be small compared to typical spin and nutation periods; otherwise, the trapezoidal approximation will produce poor results.

The deterministic algorithm estimates L_b by simultaneously solving multiple versions of Eq. (8) that arise from multiple sample intervals. The resulting overdetermined system of nonlinear equations is solved in an approximate least-squares sense. The use of multiple equations decreases the effect of noise on the accuracy of L_b. Suppose that one wants to estimate L_b using data that fall within $\pm 0.5 T_{Lb}$ s of t_k. One first determines $j_{\min} =$ [the minimum j such that $(t_k - 0.5T_{Lb}) \le t_j$] and $j_{\max} =$ [the maximum j such that $t_{j+1} \le (t_k + 0.5T_{Lb})$]. Next, one solves the following overdetermined system of quadratic equations in a least-squares sense:

$$\boldsymbol{c}_{\text{big}} L_b^2 + \boldsymbol{d}_{\text{big}} L_b + \boldsymbol{e}_{\text{big}} = 0 \tag{10}$$

where the vectors $\boldsymbol{c}_{\text{big}}$, $\boldsymbol{d}_{\text{big}}$, and $\boldsymbol{e}_{\text{big}}$ are defined by

$$\boldsymbol{c}_{\text{big}} = \left[\boldsymbol{c}_{j_{\min}}^T, \boldsymbol{c}_{(j_{\min}+1)}^T, \boldsymbol{c}_{(j_{\min}+2)}^T, \ldots, \boldsymbol{c}_{j_{\max}}^T\right]^T \tag{11a}$$

$$\boldsymbol{d}_{\text{big}} = \left[\boldsymbol{d}_{j_{\min}}^T, \boldsymbol{d}_{(j_{\min}+1)}^T, \boldsymbol{d}_{(j_{\min}+2)}^T, \ldots, \boldsymbol{d}_{j_{\max}}^T\right]^T \tag{11b}$$

$$\boldsymbol{e}_{\text{big}} = \left[\boldsymbol{e}_{j_{\min}}^T, \boldsymbol{e}_{(j_{\min}+1)}^T, \boldsymbol{e}_{(j_{\min}+2)}^T, \ldots, \boldsymbol{e}_{j_{\max}}^T\right]^T \tag{11c}$$

The weighted least-squares solution of Eq. (10) minimizes the following cost function:

$$J(L_b) = \tfrac{1}{2}\left(\boldsymbol{c}_{\text{big}} L_b^2 + \boldsymbol{d}_{\text{big}} L_b + \boldsymbol{e}_{\text{big}}\right)^T P_{\text{big}}^{-1}\left(\boldsymbol{c}_{\text{big}} L_b^2 + \boldsymbol{d}_{\text{big}} L_b + \boldsymbol{e}_{\text{big}}\right) \tag{12}$$

The positive-definite weighting matrix P_{big}^{-1} has been chosen to equal the inverse covariance of a statistical error model for Eq. (10). In this case, the cost function $J(L_b)$ can be viewed as the negative of a log-likelihood function and the minimizing L_b as a maximum likelihood estimate.

The matrix P_{big} models the correlations between the errors in Eq. (8) for the sample intervals $k = j_{\min}$ to $k = j_{\max}$. There are correlations among the components of the error vector for a given sample index k, and there are correlations with the errors of the neighboring sample intervals $k-1$ and $k+1$. The covariance matrix takes the following block tridiagonal form:

$$P_{\text{big}} = \begin{bmatrix} P_{j_{\min}} & Q_{j_{\min}} & 0 & 0 & \cdots & 0 \\ Q_{j_{\min}}^T & P_{(j_{\min}+1)} & Q_{(j_{\min}+1)} & 0 & \cdots & 0 \\ 0 & Q_{(j_{\min}+1)}^T & P_{(j_{\min}+2)} & Q_{(j_{\min}+2)} & \cdots & 0 \\ 0 & 0 & Q_{(j_{\min}+2)}^T & P_{(j_{\min}+3)} & \cdots & 0 \\ \vdots & \vdots & \vdots & \vdots & \ddots & \vdots \\ 0 & 0 & 0 & 0 & \cdots & P_{j_{\max}} \end{bmatrix} \tag{13}$$

where

$$P_k = P_{\text{true}(k)} + \{0.001 \operatorname{tr}[P_{\text{true}(k)}]\} I \tag{14a}$$

$$\begin{aligned}P_{\text{true}(k)} = {} & \sigma^2[I + 0.5\Delta t_k C_{k+1}][I - D_{k+1}][I - D_{k+1}]^T \\ & \times [I + 0.5\Delta t_k C_{k+1}]^T + \sigma^2[-I + 0.5\Delta t_k C_k][I - D_k] \\ & \times [I - D_k]^T[-I + 0.5\Delta t_k C_k]^T\end{aligned} \tag{14b}$$

$$\begin{aligned}Q_k = {} & \sigma^2[I + 0.5\Delta t_k C_{k+1}][I - D_{k+1}][I - D_{k+1}]^T \\ & \times [-I + 0.5\Delta t_{k+1} C_{k+1}]^T\end{aligned} \tag{14c}$$

are 3×3 covariance and cross-correlation matrices. The quantity σ is the standard deviation of the errors in the two components of $\hat{\boldsymbol{b}}_k$ that are perpendicular to $\hat{\boldsymbol{b}}_k$. The two 3×3 matrices C_k and D_k that appear in Eqs. (14b) and (14c) are defined as follows:

$$C_k = I_m^{-1}(-[\{I_m \boldsymbol{\gamma}_k + \boldsymbol{h}(t_k)\}\times] + [\boldsymbol{\gamma}_k \times] I_m) \tag{15a}$$

$$D_k = \hat{\boldsymbol{b}}_k \hat{\boldsymbol{b}}_k^T I_m \big/ \hat{\boldsymbol{b}}_k^T I_m \hat{\boldsymbol{b}}_k \tag{15b}$$

where the notation $[\boldsymbol{z}\times]$ indicates the 3×3 cross-product equivalent matrix that is associated with the three-dimensional vector $\boldsymbol{z}$. The ad hoc trace term in Eq. (14a) enforces positive definiteness so that P_{big}^{-1} will exist. Without this modification, P_{big} fails to be positive definite because the underlying Euler's equation has zero error in the $\hat{\boldsymbol{b}}$ direction due to the use of Eq. (3).

The error covariance model in Eqs. (13–15b) assumes that the dominant errors are those of the "measured" magnetic field direction time derivative $\hat{\dot{\boldsymbol{b}}}_k$. The error model assumes that $\sigma^2[I - \hat{\boldsymbol{b}}_k \hat{\boldsymbol{b}}_k^T]$ is the covariance matrix of the noise in $\hat{\dot{\boldsymbol{b}}}_k$. These errors propagate into Eq. (8) through their effects on $\boldsymbol{\gamma}_k$ of Eq. (7a). The resulting net error in Eq. (8) includes linear noise terms from the linear $\boldsymbol{\gamma}_k$ and $\boldsymbol{\gamma}_{k+1}$ terms in the $\boldsymbol{e}_k$ formula of Eq. (9c), quadratic noise terms from the quadratic $\boldsymbol{\gamma}_k$ and $\boldsymbol{\gamma}_{k+1}$ terms in $\boldsymbol{e}_k$, and noise that multiplies L_b from the linear $\boldsymbol{\gamma}_k$ and $\boldsymbol{\gamma}_{k+1}$ terms in the Eq. (9b) formula for $\boldsymbol{d}_k$. Only the linear noise terms have been used in the covariance model because the other two noise types are difficult to manipulate.

It is possible to use an alternate weighting matrix in the least-squares cost function of Eq. (12). The already defined P_{big}^{-1} weighting matrix is the best of several alternative weightings that have been tried for the attitude rate estimation case that is reported in Sec. VI. Alternate weighting matrices might work better in different situations.

D. Global Solution of the Least-Squares Problem

The global minimum of the least-squares cost function in Eq. (12) can be computed analytically. The cost function reduces to a quartic polynomial in L_b

$$J(L_b) = a_4 L_b^4 + a_3 L_b^3 + a_2 L_b^2 + a_1 L_b + a_0 \tag{16}$$

whose coefficients are

$$\begin{aligned} a_4 &= \tfrac{1}{2}\boldsymbol{c}_{\text{big}}^T P_{\text{big}}^{-1} \boldsymbol{c}_{\text{big}}, \qquad a_3 = \boldsymbol{d}_{\text{big}}^T P_{\text{big}}^{-1} \boldsymbol{c}_{\text{big}} \\ a_2 &= \boldsymbol{e}_{\text{big}}^T P_{\text{big}}^{-1} \boldsymbol{c}_{\text{big}} + \tfrac{1}{2}\boldsymbol{d}_{\text{big}}^T P_{\text{big}}^{-1} \boldsymbol{d}_{\text{big}} \\ a_1 &= \boldsymbol{e}_{\text{big}}^T P_{\text{big}}^{-1} \boldsymbol{d}_{\text{big}}, \qquad a_0 = \tfrac{1}{2}\boldsymbol{e}_{\text{big}}^T P_{\text{big}}^{-1} \boldsymbol{e}_{\text{big}} \end{aligned} \tag{17}$$

The global minimum of this function can be computed by solving the first-order necessary condition for an optimum:

$$0 = \frac{\mathrm{d}J}{\mathrm{d}L_b} = 4a_4 L_b^3 + 3a_3 L_b^2 + 2a_2 L_b + a_1 \tag{18}$$

Any cubic polynomial can be solved analytically. It may have only one real solution, or it may have three real solutions. One of the real roots is guaranteed to be the global minimum of the least-squares problem because $a_4 > 0$. If there is just one real solution to Eq. (18), then it is the optimal L_b estimate. If there are three real solutions, then one is the global minimum of $J(L_b)$, one is a local minimum, and one is a local maximum. The local maximum lies between the local minimum and the global minimum. The values of $J(L_b)$ at the two extreme real solutions can be used to evaluate which of them is the global minimum.

The global minimum of $J(L_b)$ might not yield the best attitude rate estimate if there is a second local minimum of the cost function. This can occur because of measurement noise and modeling error effects. Such a situation indeed occurs in some of the experimental data that are discussed in Sec. VI. In this case, it may be wise to use both solutions to initialize the angular rate estimates of two alternate runs of the Kalman filter that will be described in Sec. V. The better solution can be determined by examining the Kalman filter's behavior for the two cases.

IV. Observability Analysis

This analysis determines the conditions under which the attitude rate is observable. If the deterministic algorithm has a unique solution or, at worst, two possible distinct solutions, then the attitude rate is observable.

The observability analysis works with a modified version of the Sec. III least-squares problem. This modified problem uses the differential form of Euler's equation. It uses Eqs. (6–7b) and their time derivatives to replace $\boldsymbol{\omega}$ and $\dot{\boldsymbol{\omega}}$ with expressions involving L_b, I_m, $\boldsymbol{h}$, $\dot{\boldsymbol{h}}$, $\hat{\boldsymbol{b}}$, $\dot{\hat{\boldsymbol{b}}}$, and $\ddot{\hat{\boldsymbol{b}}}$. The resulting overdetermined system of equations for L_b takes the form

$$\bar{\boldsymbol{c}} L_b^2 + \bar{\boldsymbol{d}} L_b + \bar{\boldsymbol{e}} = 0 \tag{19}$$

where the vectors $\bar{\boldsymbol{c}}$ and $\bar{\boldsymbol{d}}$ are defined by

$$\bar{\boldsymbol{c}} = \frac{\hat{\boldsymbol{b}} \times (I_m \hat{\boldsymbol{b}})}{\left(\hat{\boldsymbol{b}}^T I_m \hat{\boldsymbol{b}}\right)^2} \tag{20a}$$

$$\bar{\boldsymbol{d}} = \left[\frac{(I + \hat{\boldsymbol{b}}\hat{\boldsymbol{b}}^T) I_m}{\hat{\boldsymbol{b}}^T I_m \hat{\boldsymbol{b}}} - \frac{2 I_m \hat{\boldsymbol{b}}\hat{\boldsymbol{b}}^T I_m}{\left(\hat{\boldsymbol{b}}^T I_m \hat{\boldsymbol{b}}\right)^2} - I\right]\dot{\hat{\boldsymbol{b}}} + \left[\frac{\hat{\boldsymbol{b}}}{\hat{\boldsymbol{b}}^T I_m \hat{\boldsymbol{b}}}\right] \times \left\{\left[I - \frac{2 I_m \hat{\boldsymbol{b}}\hat{\boldsymbol{b}}^T}{\hat{\boldsymbol{b}}^T I_m \hat{\boldsymbol{b}}}\right][I_m(\dot{\hat{\boldsymbol{b}}} \times \hat{\boldsymbol{b}}) + \boldsymbol{h}]\right\} \tag{20b}$$

The system is observable if $\bar{\boldsymbol{c}} \neq 0$ or $\bar{\boldsymbol{d}} \neq 0$ because Eq. (19) has a unique least-squares solution, or at most two distinct local minima, if either of these conditions holds. The system is unobservable if and only if $\bar{\boldsymbol{c}} = 0$ and $\bar{\boldsymbol{d}} = 0$ for all time. The condition $\bar{\boldsymbol{c}} = 0$ implies that $\hat{\boldsymbol{b}} \times (I_m \hat{\boldsymbol{b}}) = 0$. This, in turn, implies that $\hat{\boldsymbol{b}}$ is an eigenvector of I_m: $I_m \hat{\boldsymbol{b}} = \lambda \hat{\boldsymbol{b}}$ for some positive scalar eigenvalue λ. Unobservability also implies that $\dot{\bar{\boldsymbol{c}}} = 0$. This condition can be used to derive the requirement that $I_m \dot{\hat{\boldsymbol{b}}} = \lambda \dot{\hat{\boldsymbol{b}}}$, which is true if $\dot{\hat{\boldsymbol{b}}} = 0$ or if $\dot{\hat{\boldsymbol{b}}}$ is also an eigenvector of I_m with eigenvalue λ. If $\dot{\hat{\boldsymbol{b}}} \neq 0$, then I_m must have two identical eigenvalues equal to λ because $\dot{\hat{\boldsymbol{b}}}$ is perpendicular to $\hat{\boldsymbol{b}}$.

An additional condition for unobservability can be deduced by setting $\bar{\boldsymbol{d}}$ in Eq. (20b) equal to zero. First, the conditions that result from the equations $\bar{\boldsymbol{c}} = 0$ and $\dot{\bar{\boldsymbol{c}}} = 0$ can be used to simplify $\bar{\boldsymbol{d}}$ to the following form:

$$\bar{\boldsymbol{d}} = \left[\hat{\boldsymbol{b}} \Big/ \hat{\boldsymbol{b}}^T I_m \hat{\boldsymbol{b}}\right] \times [I_m(\dot{\hat{\boldsymbol{b}}} \times \hat{\boldsymbol{b}}) + \boldsymbol{h}] \tag{21}$$

By the use of Eq. (4), the angular momentum vector can be written as $\boldsymbol{L} = I_m(\alpha \hat{\boldsymbol{b}} + \hat{\boldsymbol{b}} \times \dot{\hat{\boldsymbol{b}}}) + \boldsymbol{h}$. The $\bar{\boldsymbol{c}} = 0$ condition that $\hat{\boldsymbol{b}}$ must be an eigenvector of I_m can be used to simplify this expression to yield $\boldsymbol{L} = \lambda\alpha \hat{\boldsymbol{b}} + I_m(\hat{\boldsymbol{b}} \times \dot{\hat{\boldsymbol{b}}}) + \boldsymbol{h}$. This expression and Eq. (21) can be combined to prove that $\hat{\boldsymbol{b}} \times \boldsymbol{L} = 0$ if and only if $\bar{\boldsymbol{d}} = 0$. This implies that the angular momentum vector must be parallel to the magnetic field vector for the system to be unobservable.

In summary, two conditions must hold for the attitude rate vector to be unobservable. First, the magnetic field vector must be aligned with a principal axis of inertia of the spacecraft. Second, the magnetic field vector and the angular momentum vector must be aligned with each other. The former condition implies that the magnetic field vector must be fixed in spacecraft coordinates or that the spacecraft must have at least two equal moments of inertia so that the time-varying $\hat{\boldsymbol{b}}$ vector can remain an eigenvector of I_m. The main point of this analysis is that the conditions for unobservability are very restrictive. Therefore, they are unlikely to hold true, and the algorithms of this paper can be used to deduce attitude rate in almost all cases.

V. EKF Design

The other attitude rate estimation algorithm of this paper is an EKF. The deterministic algorithm can give a rough initial estimate of the attitude rate that properly accounts for all problem nonlinearities. This estimate can be used as the initial estimate of the EKF to minimize the risks of filter divergence. The EKF can then operate on the data to produce a refined attitude rate estimate that takes better account of measurement and dynamic model errors and that operates in an efficient recursive manner.

A. Single-Stage EKF Problem Model

The EKF has been designed by modifying the nonlinear square-root information filter (SRIF) of Ref. 10, which is an extension of the linear filter of Ref. 11. One modification enables it to incorporate properly the dynamic model of the measured magnetic field direction vector, Eq. (2). Another change deals with the field direction measurements' normalization constraint.

The modified SRIF operates recursively from one measurement sample to the next. It approximately solves the following constrained, weighted nonlinear least-squares problem.

Find

$$\boldsymbol{x}_k, \boldsymbol{x}_{k+1}, \qquad \boldsymbol{\nu}_k, \boldsymbol{\nu}_{k+1}, \qquad \text{and} \qquad \boldsymbol{w}_k \tag{22a}$$

to minimize

$$J = \frac{1}{2}\left\{\left\| R_{ww(k)} \boldsymbol{w}_k \right\|^2 + \left\| \begin{bmatrix} R^+_{vv(k)} & R^+_{vx(k)} \\ 0 & R^+_{xx(k)} \end{bmatrix} \begin{bmatrix} \left(\boldsymbol{\nu}_k - \boldsymbol{\nu}_k^+\right) \\ \left(\boldsymbol{x}_k - \boldsymbol{x}_k^+\right) \end{bmatrix} \right\|^2 + \left\| R_{vv(k+1)} \boldsymbol{\nu}_{k+1} \right\|^2 \right\} \tag{22b}$$

subject to

$$A(\boldsymbol{\nu}_{k+1}, \hat{\boldsymbol{b}}_{k+1}) \hat{\boldsymbol{b}}_{k+1} = \boldsymbol{f}_b[A(\boldsymbol{\nu}_k, \hat{\boldsymbol{b}}_k)\hat{\boldsymbol{b}}_k, \boldsymbol{x}_k, \boldsymbol{w}_k, t_k, t_{k+1}] \tag{22c}$$

$$\boldsymbol{x}_{k+1} = \boldsymbol{f}_x[\boldsymbol{x}_k, \boldsymbol{w}_k, t_k, t_{k+1}] \tag{22d}$$

This problem includes the propagation from measurement sample time t_k to sample time t_{k+1} and the measurement update at time t_{k+1}. The vectors in this problem are defined as follows: Here, $\boldsymbol{x}_k$ and $\boldsymbol{x}_{k+1}$ are filter state vectors at the times t_k and t_{k+1}, $\boldsymbol{\nu}_k$ and $\boldsymbol{\nu}_{k+1}$ are two-dimensional magnetic field direction measurement error vectors at times t_k and t_{k+1}, and $\boldsymbol{w}_k$ is the discrete-time process noise that acts from time t_k to time t_{k+1}. The vectors $\boldsymbol{x}_k^+$ and $\boldsymbol{\nu}_k^+$ are a posteriori estimates of $\boldsymbol{x}_k$ and $\boldsymbol{\nu}_k$ at time t_k. The vectors $\hat{\boldsymbol{b}}_k$ and $\hat{\boldsymbol{b}}_{k+1}$ are the raw measured magnetic field direction vectors in spacecraft coordinates at times t_k and t_{k+1}.

The filter state vector $\boldsymbol{x}$ is eight-dimensional. It consists of the 3×1 angular rate vector and corrections to five of the six inertia matrix elements:

$$\boldsymbol{x} = \left[\boldsymbol{\omega}^T, \Delta I_{mxx}, \Delta I_{mxy}, \Delta I_{mxz}, \Delta I_{myy}, \Delta I_{myz}\right]^T \tag{23}$$

The true inertia matrix is the sum of a nominal value I_{m0} and a correction term,

$$I_m = I_{m0} + \begin{bmatrix} \Delta I_{mxx} & \Delta I_{mxy} & \Delta I_{mxz} \\ \Delta I_{mxy} & \Delta I_{myy} & \Delta I_{myz} \\ \Delta I_{mxz} & \Delta I_{myz} & 0 \end{bmatrix} \tag{24}$$

In this case, the inertia about the nominal spin axis is assumed to be known exactly to make the other five inertia matrix elements observable. This element was chosen because it is roughly equal to the minimum principal inertia. Such a choice helps to avoid the possibility of a singular inertia matrix estimate.

The two vector functions $\boldsymbol{f}_b$ and $\boldsymbol{f}_x$ in Eqs. (22c) and (22d) constitute the filter's discrete-time dynamics model. The three-dimensional vector function $\boldsymbol{f}_b[A(\boldsymbol{\nu}_k, \hat{\boldsymbol{b}}_k)\hat{\boldsymbol{b}}_k, \boldsymbol{x}_k, \boldsymbol{w}_k, t_k, t_{k+1}]$ computes a magnetic field direction at time t_{k+1} by numerically integrating the magnetic field differential equation (2), starting from the initial condition $\hat{\boldsymbol{b}}(t_k) = A(\boldsymbol{\nu}_k, \hat{\boldsymbol{b}}_k)\hat{\boldsymbol{b}}_k$. The first three elements of the

eight-dimensional vector function $\boldsymbol{f}_x[\boldsymbol{x}_k, \boldsymbol{w}_k, t_k, t_{k+1}]$ propagate the angular rate vector $\boldsymbol{\omega}(t)$ from time t_k to time t_{k+1} via numerical integration of the attitude dynamics differential equation (1). This integration starts by initializing $\boldsymbol{\omega}(t_k)$ to equal the first three elements of $\boldsymbol{x}_k$. It uses the inertia matrix in Eq. (24) with perturbations as defined by the last five elements of $\boldsymbol{x}_k$. The resulting $\boldsymbol{\omega}(t)$ time history also gets used in the integration of Eq. (2) that computes $\boldsymbol{f}_b$.

The process noise vector $\boldsymbol{w}_k$ consists of the magnetic field inertial rate in Eq. (2) and the disturbance torque in Eq. (1). These quantities are defined during the numerical integration interval $t_k \le t < t_{k+1}$ as follows:

$$\begin{bmatrix} \boldsymbol{w}_\omega(t) \\ \boldsymbol{w}_n(t) \end{bmatrix} = \boldsymbol{w}_k \tag{25}$$

The last five elements of the $\boldsymbol{f}_x$ function define the dynamics of the inertia matrix perturbations in $\boldsymbol{x}_k$. They are modeled as being constants. Thus, for $j = 4, 5, 6, 7$, and 8,

$$(\boldsymbol{f}_x[\boldsymbol{x}_k, \boldsymbol{w}_k, t_k, t_{k+1}])_j = (\boldsymbol{x}_k)_j \tag{26}$$

The least-squares cost function in Eq. (22b) can be interpreted as the negative of a log-likelihood function, which implies that the filter is a maximum-likelihood estimator. The weighting matrices $R_{ww(k)}$, $R^+_{vv(k)}$, $R^+_{vx(k)}$, $R^+_{xx(k)}$, and $R_{vv(k+1)}$ can be interpreted statistically. The noise/error terms $\boldsymbol{w}_k$, $(\boldsymbol{\nu}_k - \boldsymbol{\nu}^+_k)$, $(\boldsymbol{x}_k - \boldsymbol{x}^+_k)$, and $\boldsymbol{\nu}_{k+1}$ are each Gaussian, zero-mean random vectors, and the weighting matrices define their covariances and cross correlations:

$$E\left\{\boldsymbol{w}_k \boldsymbol{w}_k^T\right\} = R^{-1}_{ww(k)} R^{-T}_{ww(k)} \tag{27a}$$

$$E\left\{\left(\boldsymbol{\nu}_k - \boldsymbol{\nu}^+_k\right)\left(\boldsymbol{\nu}_k - \boldsymbol{\nu}^+_k\right)^T\right\} = \left[R^+_{vv(k)}\right]^{-1}\left(I + R^+_{vx(k)}\left[R^+_{xx(k)}\right]^{-1} \times \left[R^+_{xx(k)}\right]^{-T}\left[R^+_{vx(k)}\right]^T\right)\left[R^+_{vv(k)}\right]^{-T} \tag{27b}$$

$$E\left\{\left(\boldsymbol{\nu}_k - \boldsymbol{\nu}^+_k\right)\left(\boldsymbol{x}_k - \boldsymbol{x}^+_k\right)^T\right\} = -\left[R^+_{vv(k)}\right]^{-1} R^+_{vx(k)} \times \left[R^+_{xx(k)}\right]^{-1}\left[R^+_{xx(k)}\right]^{-T} \tag{27c}$$

$$E\left\{\left(\boldsymbol{x}_k - \boldsymbol{x}^+_k\right)\left(\boldsymbol{x}_k - \boldsymbol{x}^+_k\right)^T\right\} = \left[R^+_{xx(k)}\right]^{-1}\left[R^+_{xx(k)}\right]^{-T} \tag{27d}$$

$$E\left\{\boldsymbol{\nu}_{k+1}\boldsymbol{\nu}^T_{k+1}\right\} = \left[R_{vv(k+1)}\right]^{-1}\left[R_{vv(k+1)}\right]^{-T} \tag{27e}$$

where the superscript $-T$ indicates the transpose of the inverse of the matrix in question. The only two error vectors with a nonzero cross-correlation are $(\boldsymbol{\nu}_k - \boldsymbol{\nu}^+_k)$ and $(\boldsymbol{x}_k - \boldsymbol{x}^+_k)$. The covariances and correlations of these two vectors represent a posteriori values, that is, values based on the measurements up through $\hat{\boldsymbol{b}}_k$, which is why the associated R matrices have the plus sign superscript.

The 3×3 matrix function $A(\boldsymbol{\nu}, \hat{\boldsymbol{b}})$ in Eq. (22c) is an orthogonal coordinate transformation matrix. It uses the two elements of the $\boldsymbol{\nu}$ error vector to define a rotation quaternion about a rotation axis that is perpendicular to $\hat{\boldsymbol{b}}$:

$$\boldsymbol{q}(\boldsymbol{\nu}, \hat{\boldsymbol{b}}) = \begin{bmatrix} V(\hat{\boldsymbol{b}})\boldsymbol{\nu} \\ \sqrt{1 - \boldsymbol{\nu}^T V^T(\hat{\boldsymbol{b}}) V(\hat{\boldsymbol{b}})\boldsymbol{\nu}} \end{bmatrix} \tag{28}$$

where the 3×2 matrix $V(\hat{\boldsymbol{b}})$ is constructed so that the 3×3 matrix $[V(\hat{\boldsymbol{b}}), \hat{\boldsymbol{b}}]$ is orthogonal. The transformation $A(\boldsymbol{\nu}, \hat{\boldsymbol{b}})$ is the orthogonal matrix that is associated with $\boldsymbol{q}(\boldsymbol{\nu}, \hat{\boldsymbol{b}})$, per the equations in Ref. 12. This matrix rotates the measured magnetic field direction $\hat{\boldsymbol{b}}$ by the measurement errors to compute the "true" magnetic field direction $A(\boldsymbol{\nu}, \hat{\boldsymbol{b}})\hat{\boldsymbol{b}}$.

B. Unique Contributions of the Filter Design

The unique contributions of this filter development are in the use of the $A(\boldsymbol{\nu}, \hat{\boldsymbol{b}})$ matrix and the magnetic field propagation equation (22c). These provide a rational way for the filter to incorporate Eq. (2) into its dynamics model, which is necessary to determine the attitude rate based on the magnetic field measurements. Oshman and Dellus do this by augmenting the state vector with an estimate of $\hat{\boldsymbol{b}}$[3]. This leads to a measurement error model that has a singular covariance matrix because $\hat{\boldsymbol{b}}$ is constrained to have unit magnitude.

The present filter avoids a singular measurement error covariance by defining the two-dimensional measurement error vector $\boldsymbol{\nu}$ and the corresponding error rotation $A(\boldsymbol{\nu}, \hat{\boldsymbol{b}})$. The filter state gets augmented by the measurement error $\boldsymbol{\nu}$ rather than by the measurement $\hat{\boldsymbol{b}}$. Dynamic propagation equation (22c) uses the $\dot{\boldsymbol{b}}$ differential equation, Eq. (2), to define $\boldsymbol{f}_b$, but Eq. (22c) is effectively a propagation equation for $\boldsymbol{\nu}$ rather than a propagation equation for $\hat{\boldsymbol{b}}$. It is an implicit propagation equation, and the EKF needs to deal with this equation sensibly. The new filter's measurement equation at sample time t_{k+1} is effectively $R_{vv(k+1)}\boldsymbol{\nu}_{k+1} = \bar{\boldsymbol{\nu}}_{k+1}$, where $\bar{\boldsymbol{\nu}}_{k+1}$ is a two-dimensional Gaussian random noise vector whose mean is zero and whose covariance matrix is the identity matrix. This approach for maintaining the normalization of the measured magnetic field is akin to the multiplicative update approach for maintaining quaternion normalization in an attitude determination EKF.[13]

C. EKF Algorithm

The EKF functions like the filter of Ref. 10. It starts with a propagation of the state and the square-root information matrix from stage k to stage $k+1$. The second step is a measurement update at stage $k+1$. The process then repeats itself. The details of these steps are as follows:

1. State and Square-Root Information Matrix Propagation to Stage $k+1$

The first part of the propagation step uses the stage-k a posteriori estimates $\boldsymbol{\nu}^+_k$ and $\boldsymbol{x}^+_k$ in Eqs. (22c) and (22d) to compute a priori estimates $\boldsymbol{\nu}^-_{k+1}$ and $\boldsymbol{x}^-_{k+1}$ at stage $k+1$ along with a linearized model of Eqs. (22c) and (22d). The a priori state at stage $k+1$ is $\boldsymbol{x}^-_{k+1} = \boldsymbol{f}_x[\boldsymbol{x}^+_k, 0, t_k, t_{k+1}]$. The calculation of $\boldsymbol{\nu}^-_{k+1}$ starts with a computation of the a priori magnetic field direction estimate:

$$\hat{\boldsymbol{b}}^-_{k+1} = \boldsymbol{f}_b\left[A_k\left(\boldsymbol{\nu}^+_k, \hat{\boldsymbol{b}}_k\right)\hat{\boldsymbol{b}}_k, \boldsymbol{x}^+_k, 0, t_k, t_{k+1}\right] \tag{29}$$

Here, $\boldsymbol{\nu}^-_{k+1}$ is determined by solving $A(\boldsymbol{\nu}^-_{k+1}, \hat{\boldsymbol{b}}_{k+1})\hat{\boldsymbol{b}}_{k+1} = \hat{\boldsymbol{b}}^-_{k+1}$, where $\hat{\boldsymbol{b}}_{k+1}$ is the measured magnetic field direction vector at sample time t_{k+1}. To solve this equation, one first computes an attitude error vector and an attitude error angle:

$$\boldsymbol{e} = \hat{\boldsymbol{b}}^-_{k+1} \times \hat{\boldsymbol{b}}_{k+1} \qquad \text{and} \qquad \theta = \operatorname{atan2}\left\{\|\boldsymbol{e}\|, \left[\left(\hat{\boldsymbol{b}}^-_{k+1}\right)^T \hat{\boldsymbol{b}}_{k+1}\right]\right\} \tag{30}$$

If $\theta = 0$, then $\boldsymbol{\nu}^-_{k+1} = 0$. Otherwise, $\boldsymbol{\nu}^-_{k+1}$ is determined by solving the system of equations

$$V(\hat{\boldsymbol{b}}_{k+1})\boldsymbol{\nu}^-_{k+1} = [\sin(\theta/2)/\|\boldsymbol{e}\|]\,\boldsymbol{e} \tag{31}$$

The case $\theta = 180$ deg should never occur. Although this system of three linear equations in two unknowns is overdetermined, it is consistent and is guaranteed to have a solution.

The linearized version of Eqs. (22c) and (22d) takes the form:

$$\begin{bmatrix} \left(\boldsymbol{\nu}_{k+1} - \boldsymbol{\nu}^-_{k+1}\right) \\ \left(\boldsymbol{x}_{k+1} - \boldsymbol{x}^-_{k+1}\right) \end{bmatrix} = \begin{bmatrix} \Phi_{vvk} & \Phi_{vxk} \\ 0 & \Phi_{xxk} \end{bmatrix} \begin{bmatrix} \left(\boldsymbol{\nu}_k - \boldsymbol{\nu}^+_k\right) \\ \left(\boldsymbol{x}_k - \boldsymbol{x}^+_k\right) \end{bmatrix} + \begin{bmatrix} \Gamma_{vk} \\ \Gamma_{xk} \end{bmatrix} \boldsymbol{w}_k \tag{32}$$

where

$$\Phi_{vvk} = U_{k+1} \left.\frac{\partial \boldsymbol{f}_b}{\partial [A\hat{\boldsymbol{b}}]}\right|_k \left.\frac{\partial \left[A\left(\boldsymbol{\nu}^+_k, \hat{\boldsymbol{b}}_k\right)\hat{\boldsymbol{b}}_k\right]}{\partial \boldsymbol{\nu}^+_k}\right.$$

$$\Phi_{vxk} = U_{k+1} \left.\frac{\partial \boldsymbol{f}_b}{\partial \boldsymbol{x}}\right|_k, \qquad \Phi_{xxk} = \left.\frac{\partial \boldsymbol{f}_x}{\partial \boldsymbol{x}}\right|_k \tag{33}$$

$$\Gamma_{vk} = U_{k+1} \left.\frac{\partial \boldsymbol{f}_b}{\partial \boldsymbol{w}}\right|_k, \qquad \Gamma_{xk} = \left.\frac{\partial \boldsymbol{f}_x}{\partial \boldsymbol{w}}\right|_k \tag{34}$$

with

$$U_{k+1} = \left\{ V^T\left(\hat{\boldsymbol{b}}_{k+1}^-\right) \frac{\partial\left[A\left(\boldsymbol{\nu}_{k+1}^-, \hat{\boldsymbol{b}}_{k+1}\right)\hat{\boldsymbol{b}}_{k+1}\right]}{\partial \boldsymbol{\nu}_{k+1}^-} \right\}^{-1} V^T\left(\hat{\boldsymbol{b}}_{k+1}^-\right) \tag{35}$$

The notation $\partial \boldsymbol{f}_b / \partial[A\hat{\boldsymbol{b}}]$ refers to differentiation of $\boldsymbol{f}_b$ with respect to its first argument, and the notation $|_k$ refers to evaluation of the corresponding derivative at the arguments $[A_k(\boldsymbol{\nu}_k^+, \hat{\boldsymbol{b}}_k)\hat{\boldsymbol{b}}_k], \boldsymbol{x}_k^+, \boldsymbol{w}_k = 0, t_k$, and t_{k+1}, whichever are appropriate. The 2×3 matrix $V^T(\hat{\boldsymbol{b}}_{k+1}^-)$ in Eq. (35) projects the corresponding linearized version of Eq. (22c) perpendicular to $\hat{\boldsymbol{b}}_{k+1}^-$.

The second part of the propagation step uses the a posteriori square-root information matrices at stage k and the linearized dynamics in Eq. (32) to compute the a priori square-root information matrices at stage $k+1$. It inverts the relationship in Eq. (32) and uses the result to eliminate $(\boldsymbol{\nu}_k - \boldsymbol{\nu}_k^+)$ and $(\boldsymbol{x}_k - \boldsymbol{x}_k^+)$ from the cost function in Eq. (22b). The first two terms of that cost function then get combined and transformed by using an orthogonal/upper-triangular (QR) factorization. These operations yield the elements of the left-hand block matrix in the following expression:

$$\begin{bmatrix} R_{ww(k)}^- & R_{wv(k+1)}^- & R_{wx(k+1)}^- \\ 0 & R_{vv(k+1)}^- & R_{vx(k+1)}^- \\ 0 & 0 & R_{xx(k+1)}^- \end{bmatrix} = T_{k+1}^- \begin{bmatrix} R_{ww(k)} & 0 & 0 \\ 0 & R_{vv(k)}^+ & R_{vx(k)}^+ \\ 0 & 0 & R_{xx(k)}^+ \end{bmatrix}$$

$$\times \begin{bmatrix} I & 0 & 0 \\ \left\{-\Phi_{vvk}^{-1}\left[\Gamma_{vk} - \Phi_{vxk}\Phi_{xxk}^{-1}\Gamma_{xk}\right]\right\} & \Phi_{vvk}^{-1} & \left\{-\Phi_{vvk}^{-1}\Phi_{vxk}\Phi_{xxk}^{-1}\right\} \\ \left\{-\Phi_{xxk}^{-1}\Gamma_{xk}\right\} & 0 & \Phi_{xxk}^{-1} \end{bmatrix} \tag{36}$$

where the orthogonal matrix T_{k+1}^- is determined during the QR factorization and causes the matrix on the left-hand side to be upper triangular. The matrices $R_{ww(k)}^-$, $R_{vv(k+1)}^-$, and $R_{xx(k+1)}^-$ are all square, upper-triangular, nonsingular matrices. They have the minus sign superscript because they are a priori square-root information matrices at stage $k+1$.

2. Measurement Update at Stage $k+1$

The measurement update combines the last term in the cost of Eq. (22b) with the transformed first two terms. It uses QR factorization to compute

$$\begin{bmatrix} R_{vv(k+1)}^+ & R_{vx(k+1)}^+ \\ 0 & R_{xx(k+1)}^+ \\ 0 & 0 \end{bmatrix} = T_{k+1}^+ \begin{bmatrix} R_{vv(k+1)}^- & R_{vx(k+1)}^- \\ 0 & R_{xx(k+1)}^- \\ R_{vv(k+1)} & 0 \end{bmatrix} \tag{37a}$$

$$\begin{bmatrix} \boldsymbol{z}_{v(k+1)}^+ \\ \boldsymbol{z}_{x(k+1)}^+ \\ \boldsymbol{z}_{res(k+1)} \end{bmatrix} = T_{k+1}^+ \begin{bmatrix} \left\{R_{vv(k+1)}^- \boldsymbol{\nu}_{k+1}^- + R_{vx(k+1)}^- \boldsymbol{x}_{k+1}^-\right\} \\ \left\{R_{xx(k+1)}^- \boldsymbol{x}_{k+1}^-\right\} \\ 0 \end{bmatrix} \tag{37b}$$

where T_{k+1}^+ is an orthogonal matrix that is determined by the QR factorization and where the matrices $R_{vv(k+1)}^+$, $R_{vx(k+1)}^+$, and $R_{xx(k+1)}^+$ constitute the a posteriori state estimation error square-root information matrix. The a posteriori state estimates $\boldsymbol{\nu}_{k+1}^+$ and $\boldsymbol{x}_{k+1}^+$ are determined by solving the following upper-triangular system of linear equations:

$$\begin{bmatrix} R_{vv(k+1)}^+ & R_{vx(k+1)}^+ \\ 0 & R_{xx(k+1)}^+ \end{bmatrix} \begin{bmatrix} \boldsymbol{\nu}_{k+1}^+ \\ \boldsymbol{x}_{k+1}^+ \end{bmatrix} = \begin{bmatrix} \boldsymbol{z}_{v(k+1)}^+ \\ \boldsymbol{z}_{x(k+1)}^+ \end{bmatrix} \tag{38}$$

The results of the measurement update prepare the filter for recursive iteration at the next stage.

3. Filter Initialization

The filter gets initialized as follows: $v_0^+ = 0$. The first three elements of $\boldsymbol{x}_0^+$ equal the rate estimate of the deterministic algorithm, and the remaining five elements of $\boldsymbol{x}_0^+$ equal zero. $R_{vv(0)}^+ = R_{vv(0)}$, and $R_{vx(0)}^+ = 0$. $R_{xx(0)}^+$ is initialized to be the square root of the inverse of the covariance of the uncertainty in the estimate $\boldsymbol{x}_0^+$. This initialization accounts for the measurement at sample time t_0. The first filter operation is dynamic propagation from sample time t_0 to sample time t_1, and the second operation is the measurement update at time t_1.

D. Linearized Observability Analysis

A linearized observability analysis can be performed on the EKF's system model. Such an analysis checks local observability. Local observability holds if there is a unique local minimum of the least-squares estimation problem that discards a priori information about the initial state and that sets the process noise to zero. Such an analysis is needed to verify the simultaneous observability of the three body-axis angular rates and the five inertia matrix perturbations.

The linearized observability analysis uses many of the same equations and operations as the EKF. The following are the two principal differences: First, $R_{xx(0)}^+$ is initialized to be 0. Second, $\boldsymbol{w}_k = 0$ is enforced, which eliminates the $\boldsymbol{w}_k$ terms from the operations that the SRIF uses to compute the a priori square-root information matrices for ν_{k+1} and $\boldsymbol{x}_{k+1}$ during its dynamic propagation. This modification eliminates the first row and the first column from each block matrix in Eq. (36). Otherwise, the observability analysis performs the same dynamic propagation and measurement update operations that the EKF performs on its square-root information matrices. It does not, however, perform vector operations to compute different estimates of $\boldsymbol{\nu}_{k+1}$ or $\boldsymbol{x}_{k+1}$. Also, it uses the EKF's linearized dynamic model, Eq. (32), and the same Φ matrices as are used in the EKF.

The observability analysis evaluates whether $\boldsymbol{x}_N$ can be uniquely determined based on the magnetic field direction vector measurements $\hat{\boldsymbol{b}}_0$ through $\hat{\boldsymbol{b}}_N$. It does this by propagating and updating its square-root information matrices starting from sample time t_0 and ending at sample time t_N. The system is locally observable if the rank of $R_{xx(N)}^+$ is eight, that is, if $R_{xx(N)}^+$ is full rank.

VI. Results

A. Experimental Data from a Spinning Sounding Rocket

The attitude rate estimation algorithms of this paper have been tested using data from the Cleft Accelerated Plasma Experimental Rocket (CAPER). CAPER was a sounding rocket that was launched in January 1999 from the Andoya Rocket Range in Norway. Its flight lasted over 1200 s. CAPER was a minor axis spin-stabilized spacecraft. It represents an interesting and challenging attitude rate estimation case because its nutation mode experienced unstable growth from an initial coning half-angle of 20 deg to a coning half-angle of more than 75 deg at the end of its flight.[9] This paper's new algorithms will be used to estimate CAPER's attitude rate from its magnetometer measurement time history, which was sampled at a nominal frequency of 4 Hz.

The estimation results of Ref. 9 are used to provide "truth" rates for purposes of evaluating the new algorithms' rate estimates. These truth rates are not completely independent because Ref. 9 also uses magnetometer data in its estimator. Nevertheless, there is a reasonable degree of independence because Ref. 9 also uses sun-sensor and horizon-crossing indicator data. These data are available during the first 75% of the flight and are sufficient to estimate attitude and rate. Furthermore, Ref. 9 uses a more accurate algorithm, a smoother, and it estimates attitude in addition to attitude rate. Although it is impossible to determine the true accuracy of the Ref. 9 truth rates, the covariance outputs of its smoother indicate a 1-σ accuracy on the order of 0.5 deg/s per axis or better. This assessment takes into account the smoother's documented conservatism vis-à-vis an independent attitude check.

B. Results for the Deterministic Algorithm

The deterministic algorithm has been tried using various input parameters. Good results have been obtained using a numerical differentiation batch interval of $T_{\text{derv}} = 1$ s to compute $\hat{\boldsymbol{b}}_k$, a least-squares estimation batch interval of $T_{Lb} = 12$ s to compute L_b, and the nominal prelaunch estimate of CAPER's moment of inertia matrix $I_m = \text{diag}(185.4, 185.4, 18.73)\ \text{kg} \cdot \text{m}^2$. CAPER's spin period ranged from 4.6 s at the start of the flight to 16.7 s at the end. The differentiation batch interval is reasonably small compared to the minimum spin period. The L_b estimation batch interval ranges from 2.6 spin periods at the beginning of the flight to 0.7 spin periods at the end, which also seems reasonable for purposes of averaging out noise effects.

Estimation results for this case are presented in Fig. 1. The horizontal axis's time datum is set to zero at the apogee of the CAPER trajectory. The solid upper curve in Fig. 1 plots the magnitude of the estimated attitude rate $\|\boldsymbol{\omega}_{\text{est}}(t)\|$ vs t, and the dotted lower curve plots the magnitude of the estimation error $\|\boldsymbol{\omega}_{\text{est}}(t) - \boldsymbol{\omega}_{\text{truth}}(t)\|$ vs t. Figure 1 shows that the attitude rate error is small for most of the data run. It hovers near 5% of the true attitude rate. This indicates excellent performance of the deterministic algorithm. During one short period, however, there is an error spike; the magnitude of the rate error jumps to more than 25% of the actual attitude rate at about 430 s before apogee.

This error spike can be explained in terms of the nonlinear least-squares cost function in Eqs. (12) and (16). As noted earlier, there can be two local minima of this quartic polynomial. The error spike on Fig. 1 corresponds to a situation in which there is a second local minimum in addition to the global minimum. If L_b for this alternate local minimum is substituted into Eq. (6) to compute ω_k, then the error spike disappears from Fig. 1. The error spike in Fig. 1 corresponds to cases in which the two local minima have least-squares costs that are close to each other, that is, their difference is less than 35% of the lower of the two costs.

One can define criteria that indicate whether the global minimum is likely to provide the best attitude rate estimate. If the global minimum is unique, then it provides the best estimate. This happens in 81% of the Fig. 1 cases. Alternatively, if the second local minimum has a cost that is at least 50% higher than the global minimum, then the global minimum can be deemed trustworthy. This is true in 89% of the two-minima cases. By these criteria, only 2% of the CAPER cases are ambiguous, and only 18% of these problem cases yield the wrong local minimum. In the cases that are not ambiguous, the deterministic algorithm achieves attitude rate estimation errors that are no greater than about 5% of the actual spin rate. In the other cases, the EKF can be used to distinguish the best solution, as will be demonstrated later in this section.

The length of the L_b estimation batch interval T_{Lb} affects the deterministic algorithm's performance. A number of runs have been done with $T_{Lb} = 6$ s instead of 12 s. These produce poorer results: There are more cases in which the minimizing L_b does not produce the best attitude rate estimate, and there is even an isolated case in which both local minima of $J(L_b)$ produce attitude rate errors of 30% or more. Thus, the longer batch interval improves the deterministic algorithm. There is probably a practical upper limit to T_{Lb}. Beyond this limit, the estimation accuracy may tend to degrade due to torque errors in the Euler dynamics model or due to violations of the assumption that the magnetic field remains fixed in inertial space.

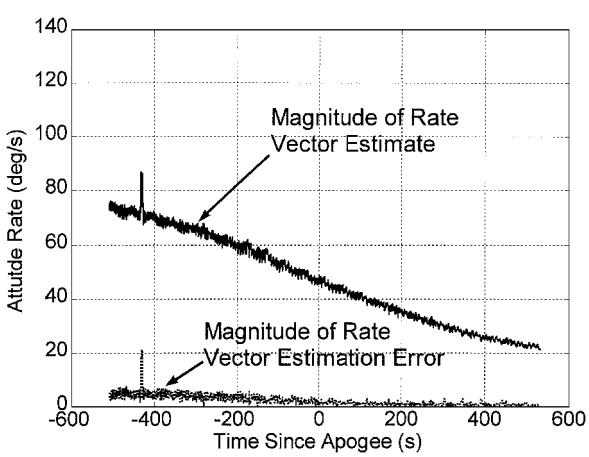

Fig. 1 Magnitude time histories of the deterministic algorithm's attitude rate vector and attitude rate error vector, a typical case.

The deterministic algorithm is somewhat insensitive to the inertia matrix estimate that gets used for I_m. The algorithm has been tried using both the prelaunch estimate of I_m and the best estimate of I_m that was produced in the study of Ref. 9. The deterministic algorithm performs similarly for both I_m estimates, although there are slightly fewer error spikes for the prelaunch I_m, which seems counterintuitive. This result may be caused by the Ref. 9 use of a CAPER dynamic model that includes flexibility effects.

C. EKF Results

The EKF of Sec. V has been tested on the CAPER data. One goal of this part of the study has been to test the filter's ability to converge from initial rate estimates that come from the deterministic algorithm. Another goal has been to test the accuracy of the EKF in comparison to that of the deterministic algorithm. A number of runs have been tried using various filter tunings and various initialization times during CAPER's flight.

The observability calculations of Sec. V have been performed during each EKF run. The matrix $R^{+}_{xx(N)}$ has been verified to be full rank in every case. Therefore, the attitude rate vector and the five inertia matrix perturbations are observable in the local linearized sense.

The EKF has been tested in a tough situation, one with significant initialization uncertainty due to the existence of two local minima of nearly equal cost in the deterministic rate estimation problem. A pair of EKF runs have been initialized at $t_0 = -433.8$ s. One run uses the initial $\boldsymbol{\omega}$ that corresponds to the deterministic algorithm's global minimum, and the other run uses the initial $\boldsymbol{\omega}$ that corresponds to the deterministic algorithm's other local minimum. At this initialization time, the global minimum yields one of the deterministic algorithm's worst initial $\boldsymbol{\omega}$ estimates, and the other local minimum yields the best initial $\boldsymbol{\omega}$ estimate. (Note again the error spike on Fig. 1.) These runs use the prelaunch estimate of the inertia matrix as the filter's nominal inertia matrix I_{m0} of Eq. (24).

The filter uses the same tuning for both of these cases. The $R_{vv(k)}$ measurement error weighting matrix equals diag(40, 40), which corresponds to 2.9 deg of $\hat{\boldsymbol{b}}$ direction error per axis. The $R_{ww(k)}$ process noise weighting matrix equals $\sqrt{(\Delta t_k)}\ \text{diag}(621, 621, 621, 4.8, 4.8, 1.5)$, where the first three entries of the diagonal matrix are in units of seconds to the 0.5 power per radian and the last three entries are in units of per Newton per meter per seconds to the 0.5 power. The upper-left 3×3 block of the filter's initial state square-root information matrix $R^{+}_{xx(0)}$ equals diag(2.9, 2.9, 2.9) s/rad, which corresponds to a 20-deg/s initial rate standard deviation per axis, consistent with the error in the poorer rate estimate from the deterministic algorithm. The lower right 5×5 block of $R^{+}_{xx(0)}$ equals the inertia matrix perturbation covariance that results from the following uniform distributions in principal inertias and principal axis orientations: $\pm 20\%$ for the principal inertias perpendicular to the nominal spin axis, ± 2 deg for the two orthogonal orientation perturbations of the spin axis direction, and ± 45 deg for the orientation perturbation about the nominal spin axis. The remaining elements of $R^{+}_{xx(0)}$ are set to zero.

Results from these Kalman filtering runs are presented in Fig. 2. Figure 2 plots the magnitude time histories of the estimated attitude rate vector and the magnitude time histories of the estimation error for the two EKF runs. These two plot types are the same as those that appear on Fig. 1 for the deterministic attitude rate estimator. It is obvious from Fig. 2 that the poor initialization yields much poorer initial performance: Notice the large initial oscillations of the solid gray curve at the top of Fig. 2 and the large initial peaks of the dashed gray curve at the bottom of Fig. 2. The curves for the good initial estimates, the two black curves, exhibit almost no initial transients. Both cases eventually converge, however, and their steady-state performance is similar.

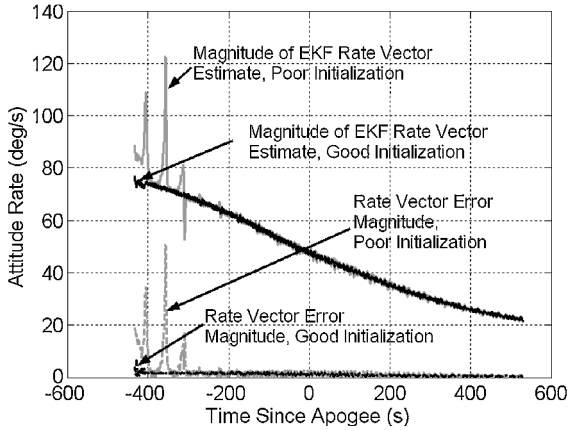

Fig. 2 EKF magnitude time histories for the attitude rate vector and the attitude rate error vector; a case with a poor initialization and a case with a good initialization.

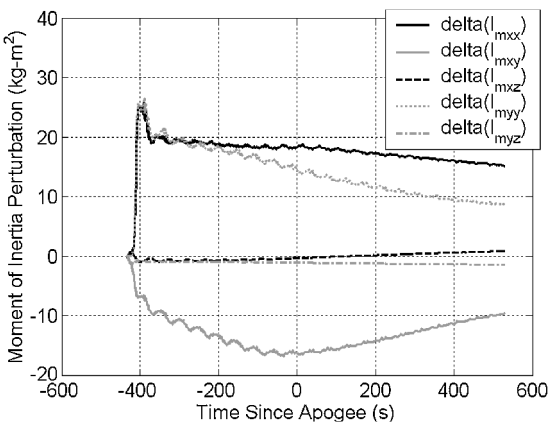

Fig. 3 Time histories of EKF estimates of inertia matrix element perturbations.

Figure 2 shows that the rate error for the good initialization starts at a magnitude of about 4 deg/s and immediately drops down to about 2 deg/s or less. By the end of the flight, the error is less than 1 deg/s. This contrasts with the deterministic algorithm's error curve in Fig. 1, which starts out oscillating between 3 and 7 deg/s, slowly decays to an average value of 2 deg/s at apogee, and continues to have peaks of about 2 deg/s near the end of the flight. Thus, the Kalman filter's tracking accuracy is superior to that of the deterministic algorithm. This level of performance is consistent with the filter's computed attitude rate estimation error covariance, which indicates that the filter's tuning is reasonable. On the other hand, the filter's estimated measurement error time history, $\boldsymbol{\nu}_0^+, \ldots, \boldsymbol{\nu}_N^+$, exhibits component standard deviations that are about 10 times smaller than the 2.9-deg-per-axis tuning value that the filter uses. Thus, there may be room for improvement in the filter's tuning.

Both initializations yield convergence in Fig. 2, but it would be preferable to use the initial rate estimate that yields smaller error transients, that is, the estimate from the deterministic algorithm's second local minimum. The superiority of this initialization can be determined from the EKF's estimated measurement error time history, $\boldsymbol{\nu}_0^+, \ldots, \boldsymbol{\nu}_N^+$. The best initialization yields initial transients in the $\boldsymbol{\nu}_k^+$ history that have significantly smaller peak values than the transients which are caused by the other initialization. Thus, the strategy for initializing the EKF is to try two parallel filters if the deterministic algorithm yields two distinct local minima of nearly equal cost. The attitude rate estimate is then chosen as the output of that filter run that yields the smallest initial transient oscillations in its $\boldsymbol{\nu}_k^+$ history.

Figure 3 illustrates the EKF's ability to estimate the inertia matrix corrections of Eq. (24). It shows the time histories of the five corrections for the filtering run that corresponds to the good initialization case of Fig. 2. Some of these correction terms undergo nearly step changes at the start of the filtering run, but, consistent with the assumption that they are constants, their rates of change tend to slow down as the filter nears the end of the data batch. The final estimated inertia matrix is closer to the Ref. 9 truth estimate than is the initial matrix I_{m0}, specifically, 77% closer as gauged by the induced matrix two-norm. Thus, the EKF does a reasonable job of estimating its inertia perturbation states.

The performance of the EKF has been evaluated using a number of different inputs. It has been initialized nearer to the end of the flight. Different tunings have been tried. Different values of I_{m0} have been used to initialize the inertia matrix estimate. The performance of the filter is not affected significantly by such changes. A slowing of the filter produces modest accuracy improvements in the $\boldsymbol{\omega}(t)$ estimate. This slowing is achieved by an increase in the elements of the $R_{ww(k)}$ matrix. An improved value of I_{m0} reduces the magnitudes of the inertia correction transients. Initialization of the filter with angular rate estimates from the deterministic algorithm always produces excellent performance, except for the case noted in Fig. 2, which corresponds to the error spike in Fig. 1.

A surprising aspect of these results is that the EKF works well using a rigid-body model of the spacecraft. The main point of Ref. 9 is that a rigid-body model is inadequate for attitude estimation for the CAPER mission because of the presence of significant flexible body effects. One might think that the present results contradict those of Ref. 9. This seeming discrepancy is easily resolved, however. The Ref. 9 difficulty with a rigid-body model stems from its filter/smoother estimating both attitude rate and attitude. The current filter only estimates attitude rate. If one integrates the difference between the two studies' attitude rate estimates, then one quickly builds up attitude errors of 20 deg and more. This is far more error than was noted for the attitude estimates of Ref. 9. The current filter is able to achieve reasonable attitude rate estimation performance because it can tolerate small rate errors that are caused by the inaccuracy of its rigid-body model. The filter/smoother of Ref. 9 does not have this luxury because these small rate errors integrate to become excessively large attitude errors.

VII. Conclusions

Two new attitude rate estimation algorithms have been developed for use on spacecraft, a deterministic algorithm and an EKF. Both of them work with a time series of Earth magnetic field direction measurements from a magnetometer, and both use Euler's equation for the attitude dynamics of a rigid body with momentum wheels. The deterministic algorithm uses the kinematic equation for the Earth's magnetic field direction in spacecraft coordinates to estimate the two components of the spin rate that are perpendicular to the magnetic field. It uses Euler's equation to solve for the remaining component via a global nonlinear least-squares batch estimation technique. The EKF estimates the attitude rate and perturbations to five of the spacecraft's six inertia matrix elements. It works with Euler's equation and the magnetic field kinematics equation and includes measurement error states. The propagation procedure for these error states uses multiplicative-type operations.

These two algorithms have been evaluated using flight data from a spinning sounding rocket whose spin rate started at 78 deg/s and decayed to 20 deg/s by the end of the flight. The deterministic algorithm achieves accuracies ranging from 7 deg/s at the start of the flight down to 2 deg/s near the end, except in unusual cases when its nonlinear least-squares solver picks a wrong local minimum. Convergence of the EKF can be ensured by using the deterministic algorithm's output to initialize the filter's rate estimate. The filter's measurement error estimates can be used to distinguish between good and bad initializations in cases where the deterministic algorithm yields two distinct local minima. The EKF's accuracy ranges from 2 deg/s at the start of the flight to better than 1 deg/s at the end.

Acknowledgments

This work was supported in part by the Lady Davis Trust through a fellowship that allowed Mark Psiaki to work with the Aerospace Engineering Faculty at the Technion—Israel Institute of Technology in Haifa, Israel and in part by U.S. Air Force Office of Scientific Research Grant F49620-01-1-0117. Marc Jacobs was the Grant

Monitor. Yaakov Oshman gratefully acknowledges support from the Asher Space Research Fund.

References

[1]Azor, R., Bar-Itzhack, I. Y., and Harman, R. R., "Satellite Angular Rate Estimation from Vector Measurements," *Journal of Guidance, Control, and Dynamics*, Vol. 21, No. 3, 1998, pp. 450–457.

[2]Harman, R. R., and Bar-Itzhack, I. Y., "Pseudolinear and State-Dependent Riccati Equation Filters for Angular Rate Estimation," *Journal of Guidance, Control, and Dynamics*, Vol. 22, No. 5, 1999, pp. 723–725.

[3]Oshman, Y., and Dellus, F., "Fast Estimation of Spacecraft Angular Velocity from Sequential Geomagnetic Field Observations," *Proceedings of the AIAA/AAS Astrodynamics Specialists Conference*, AIAA, Reston, VA, 2000, pp. 322–330.

[4]Azor, R., Bar-Itzhack, I. Y., Deutschmann, J. K., and Harman, R. R., "Angular Rate Estimation Using Delayed Quaternion Measurements," *Journal of Guidance, Control, and Dynamics*, Vol. 24, No. 3, 2001, pp. 436–443.

[5]Bar-Itzhack, I. Y., "Classification of Algorithms for Angular Velocity Estimation," *Journal of Guidance, Control, and Dynamics*, Vol. 24, No. 2, 2001, pp. 214–218.

[6]Challa, M., Kotaru, S., and Natanson, G., "Magnetometer-Only Attitude and Rate Estimates During the Earth Radiation Budget Satellite 1987 Control Anomaly," *Proceedings of the AIAA Guidance, Navigation, and Control Conference*, Vol. 2, AIAA, Reston, VA, 1997, pp. 830–840.

[7]Challa, M., Natanson, G., and Ottenstein, N., "Magnetometer-Only Attitude and Rates for Spinning Spacecraft," *Proceedings of the AIAA/AAS Astrodynamics Specialists Conference*, AIAA, Reston, VA, 2000, pp. 311–321.

[8]Psiaki, M. L., Martel, F., and Pal, P. K., "Three-Axis Attitude Determination via Kalman Filtering of Magnetometer Data," *Journal of Guidance, Control, and Dynamics*, Vol. 13, No. 3, 1990, pp. 506–514.

[9]Psiaki, M. L., Klatt, E. M., Kintner, P. M., and Powell, S. P., "Attitude Estimation for a Flexible Spacecraft in an Unstable Spin," *Journal of Guidance, Control, and Dynamics*, Vol. 25, No. 1, 2002, pp. 88–95.

[10]Psiaki, M. L., Theiler, J., Bloch, J., Ryan, S., Dill, R. W., and Warner, R. E. "ALEXIS Spacecraft Attitude Reconstruction with Thermal/Flexible Motions Due to Launch Damage," *Journal of Guidance, Control, and Dynamics*, Vol. 20, No. 5, 1997, pp. 1033–1041.

[11]Bierman, G. J., *Factorization Methods for Discrete Sequential Estimation*, Academic Press, New York, 1977, pp. 69–76, 115–122.

[12]Wertz, J. R. (ed.), *Spacecraft Attitude Determination and Control*, D. Reidel, Boston, 1978, p. 414.

[13]Lefferts, E. J., Markley, F. L., and Shuster, M. D., "Kalman Filtering for Spacecraft Attitude Estimation," *Journal of Guidance, Control, and Dynamics*, Vol. 5, No. 5, 1982, pp. 417–429.